Received 10 November 2022; revised 14 December 2022; accepted 19 December 2022. Date of publication 26 December 2022; date of current version 23 January 2023.

Digital Object Identifier 10.1109/OJAP.2022.3231892

Wideband Substrate Integrated Cavity-Backed Dielectric Resonator Antenna at Sub-6-GHz Band

REZA SHAMSAEE MALFAJANI (Graduate Student Member, IEEE), JEAN-JACQUES LAURIN (Senior Member, IEEE), AND MOHAMMAD S. SHARAWI (Senior Member, IEEE)

Department of Electrical Engineering, Polytechnique Montréal, Montreal, QC H3T 1J4, Canada

CORRESPONDING AUTHOR: R. SHAMSAEE MALFAJANI (e-mail: r.shamsaee@polymtl.ca)

This work was supported by the Fonds de recherche du Québec Nature et technologies (FRQNT) under Grant 2022-PR-298793.

ABSTRACT The design and implementation of a wideband single-mode dielectric resonator antenna (DRA) with a substrate integrated cavity-backed structure is presented in this paper. Two short-circuited striplines with differential feeding are placed inside the substrate integrated cavity (SIC) for pure mode excitation of the DRA, providing stable radiation characteristics, and low cross polarization levels. The cavity is coupled to the cylindrical DRA through an annular slot. The fundamental $HEM_{11\delta}$ mode of the DRA is excited over a wide frequency band, as a result of the similar field distribution created on the coupling annular slot by two modes inside the cavity. Measurement results show a maximum gain of 8.2 dBi at 5.45 GHz. The gain is 7.8 dBi at the center frequency of 5.15 GHz and its 1-dB bandwidth is 23%. The measured 10-dB return loss bandwidth is 26% (centered at 5.15 GHz) which is the highest among the previously reported works based on cavity-backed DRAs and single-mode excited DRAs. The measured co-polarization and cross-polarization gain difference at the boresight direction is more than 26 dB. This antenna element can be used to cover a wide range of wireless standards in wireless access point and applications due to its stable wide band performance.

INDEX TERMS Cavity-backed, dielectric resonator, differential feeding, DRA antenna, substrate integrated, wideband antenna.

I. INTRODUCTION

DIELELCTRIC resonator antenna (DRA) was first investigated by Long et al. in [1]. DRAs are used in microwave and millimeter-wave bands. Different types of metallic antennas have been reported which are low profile, but exhibit narrow operation bandwidth and lower efficiency as compared to DRA antennas. DRAs are widely known for their high efficiency, wide bandwidth, low cost, and simplicity of excitation, but they are voluminous structures where their size depends on the material properties and the frequency of operation [2]. Low-profile DRAs can be made of high permittivity materials, but this increases the Q-factor [3] and consequently, reduces bandwidth. There is therefore a trade-off between the size and operating bandwidth of DRAs realized by high permittivity materials [4], [5]. Several techniques to increase DRA bandwidth were reported in the literature, such as using higher-order modes [6] and modifying DRA feed structure [7]. A hybrid feeding technique that consist of a microstrip line and a conformal strip, is also used to improve the bandwidth, as shown in [8].

Different methods for feeding DRAs were studied as well. For coupling energy into the DRA, different types of transmission lines such as microstrip line [9], [10], coaxial probe [11], coplanar waveguide [12], and substrate integrated waveguide (SIW) [13] were considered. The coupling of energy can be either with direct contact with the feeding line or a probe, or through an aperture in the DRA's underlying ground plane [14]. A substrate integrated cavity (SIC) with a slot is a good candidate for feeding the DRA when a high-quality factor is needed [15]. SIC backed slot antennas are compact, easy to fabricate, low cost, and have a high radiation efficiency. However, their narrow operating bandwidths are a known drawback [22], [23]. Moreover, using

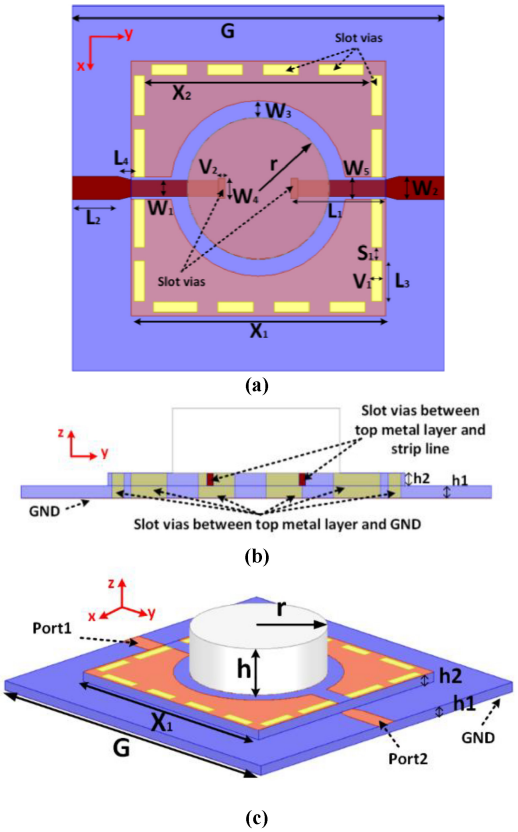

FIGURE 1. Geometry of proposed differentially fed SIC backed cDRA. (a) Top view (b) Cross-section from side view (c) Perspective view.

a method that eliminates the soldering inside the cavity is preferred for DRA feeding [24].

Differential feeding has a good compatibility with monolithic microwave integrated circuits (MMICs) and helps in generating stable radiation patterns over the frequency. More importantly, it provides symmetry in the current/field distributions, which is decreasing the cross polarization of antennas [16], [17]. With differential feeding of DRAs, unwanted modes can be suppressed inside the dielectric resonator [18], resulting in a pure mode excitation.

Several DRAs with differential feeding have been proposed for single-mode excited DRAs [9], [10], [17], [19], [20], [21], but their 1-dB gain bandwidths and their impedance bandwidths are relatively narrow. In [9], two parallel microstrip lines in a differential feeding are used for exciting the fundamental $TE_{\delta 11}$ mode inside a rectangular DRA. The measured 10-dB return loss bandwidth is 22%, centered at 2.4 GHz, and the gain varies between 3.8 and 6.6 dBi over the specified band. In [19], a rectangular DRA with the fundamental TE_{111} mode is differentially excited by a pair of conducting strips and an impedance bandwidth of 3.2% is obtained.

Growing wireless data traffic and demand for high data rate communications shift the frequency of communication to higher frequencies searching for more bandwidth. The sub-6 GHz bands (1.8 – 6 GHz) of the fifth generation (5G) wireless standards are desirable because they are more immune to fading and propagation loss but the design of wideband antennas is challenging at this band. In this paper, a differentially-fed SIC backed DRA with wide bandwidth and low cross polarization is proposed for sub-6 GHz communication systems. In the proposed structure, the advantages of both SIC and differentially fed slots constructed on cavities were leveraged to realize the excitation of a DRA antenna with a pure mode over a wide bandwidth, leading to obtain a stable wideband gain pattern. A differential-to-single-ended conversion scheme was integrated in the feed of the antenna to differentially excite the cavity and slot while the antenna feed is single-ended, eliminating the need for an external balun in order to save space and reduce the complexity. The SIC exhibits two modes within the band of interest and these two modes exhibit the similar field distribution on the coupling slot resulting in a constant field feeding the DRA over the band. With this feed, the mode of the DRA is $HEM_{11\delta}$ over the entire band and thus the DRA in single-mode with stable radiation characteristics (gain pattern and polarization) versus frequency. Compared to the previous single-mode DRAs, the proposed antenna shows the largest 1-dB gain and 10-dB impedance bandwidth. Measured results show a 26% 10-dB return loss bandwidth and 1-dB gain bandwidth of 23%. Over the operation band, from 4.5 to 5.8 GHz, the radiation efficiency is better than 95%.

The paper is organized as follows. The design of a SIC-backed DRA with differential feeding is described in Section II. The scheme for deferentially feeding of the DRA with a single-ended cavity feed is given in Section III. The cavity and DRA modes are discussed in Section IV. The measurement and simulation results are provided and discussed in Section V. Concluding remarks are given in Section VI.

II. DESIGN OF A SUBSTRATE INTEGRATED CAVITY-BACKED DIELECTRIC RESONATOR ANTENNA WITH DIFFERENTIAL FEEDING

In this section, we propose the design of a DRA excited by a differentially excited SIC cavity, with the goal of achieving wide bandwidth and low cross polarization. Fig. 1 shows the proposed slot-coupled cylindrical DRA backed by a substrate integrated square cavity. The structure includes two striplines inside the cavity, shorted to the top metal layer using two vias. While differentially fed, the short-circuited striplines excite the annular slot on the top metal layer of the cavity and hence the cylindrical DRA on top of the cavity. As discussed later is this section, the cavity is excited by two different modes over the operating band.

These two cavity modes generate very similar fields at the location of coupling to the DRA in the annular slot, hence a single mode ($HEM_{11\delta}$) is generated in the DRA over the entire operation band. As a result of dual-mode operation of the cavity, the antenna exhibits a wide return loss bandwidth, and since the field distribution in the coupling slot remains stable, the radiation characteristics of the antenna remain

almost constant over a wide bandwidth because of the single-mode operation of the DRA.

The design procedure starts with the selection of the dielectric resonator material as the dielectric constant of the resonator affects the bandwidth and size of the DRA antenna. In this work, the C-Stock AK from Cuming Microwave with a relative permittivity of 10 is used as the DRA material. C-Stock AK is a low-loss plastic with a loss tangent of 0.002. The large permittivity of the DRA material enables efficient coupling of power from the cavity to the DRA.

After selection of the permittivity of the DRA, an estimation of the dimensions of the cylindrical DRA (cDRA) at the center frequency of the desired band can be made. According to [25], for a cDRA with aspect ratio of r/h (where r and h are the DRA radius and height respectively), the resonant frequency of the fundamental mode ($HEM_{11\delta}$) can be approximated by:

$$f_{GHz} = \frac{(k_0 r).\ 4.7713}{h_{cm}.\left(\frac{r}{h}\right)} \quad \left(for\ 0.4 \le \frac{r}{2h} \le 6\right), \tag{1}$$

where h_{cm} is the DRA height in cm and $k_0 r$ is:

$$k_0 r = \frac{6.324}{\sqrt{\varepsilon_r + 2}}\left(0.27 + 0.36\left(\frac{r}{2h}\right) + 0.02\left(\frac{r}{2h}\right)^2\right). \tag{2}$$

Based on (1) and for the selected material, the initial values for r and h at 4.5 GHz (the lowest frequency in the desired sub-6-GHz band) are 10 mm 7.4 mm, respectively. The RO3035 substrate from Rogers (with dielectric constant and loss tangent of 3.5 and 0.0015, respectively) is selected for the construction of the cavity. This is a low-loss substrate with good mechanical properties for fabrication of multilayer structures and vias. The cavity includes two layers of RO3035 substrates with thicknesses of h_1 and h_2 (Fig. 1(b)). The upper substrate is only present at the location of the cavity (Fig. 1(c)). Two short-circuited striplines of length L_1 and width W_1 are printed on the top metal layer of the lower substrate. These striplines are shorted with slot vias (note that plated through vias can be used, but the available fabrication process required this type of plated vias) to the top metal layer of the cavity. The annular coupling slot is printed on the top metal layer of the upper substrate (Fig. 1(a)). Its inner radius and width are specified by r and W_3, respectively. The cavity is specified by parameters X_1 and X_2. X_1 is the outer dimension of the square cavity including the vias acting as side walls and X_2 is the inner dimension of the cavity, as shown in Fig. 1. The initial value for dimensions of the cavity can be determined by the waveguide cavity theory [26] at the center frequency of the desired band. Based on the cavity theory, $X2$ is set equal to one wavelength inside the substrate material at 5 GHz. Two microstrip lines (with length of L_2 and width of W_2) printed on the top layer of the lower substrate are connected to the striplines through two openings on the side walls of the cavity as shown in Fig. 1(a). The lines are differentially fed to provide differential feeding for the annular slot at the top of the cavity and generate the desired mode in the DRA.

TABLE 1. Final values of the proposed antenna with two ports.

Parameter	Value (mm)	Parameter	Value (mm)
G	54	r	10.2
X_1	36.3	h	7.75
X_2	32.3	S_1	0.8
h_1	1.524	V_1	2
h_2	1.524	V_2	0.8
W_1	2.65	L_1	12.1
W_2	3.4	W_3	1.6
W_4	3.15	L_2	8.7
W_5	3.65	L_3	5
L_4	0.15		

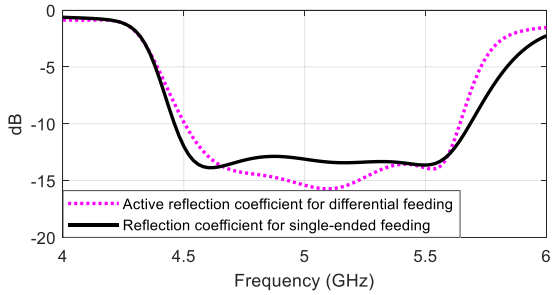

FIGURE 2. Active reflection coefficient versus frequency for the DRA antenna with SIC differential feeding (dotted line). Reflection coefficient versus frequency for the DRA antenna with SIC single-ended feeding (solid line).

In the next step with the values obtained by (1) for DRA, the short-circuited striplines and annular slot geometrical parameters (W_1, L_1, r, W_3) are optimized to get the best impedance match over the desired bandwidth. The width of the metallic slot vias (V_1 and V_2) and distance between metallic slot vias (S_1) are limited by fabrication tolerances and selected to ensure that the waves remain confined within the cavity over the operation bandwidth. The walls of the two slots and the top and bottom metal layers form a rectangular waveguide of width S_1 and height ($h = h_1 + h_2$). Considering h and S_1, The cutoff frequency of that waveguide is defined by $\frac{c}{2\times h\times\sqrt{\varepsilon_r}}$ and $\frac{c}{2\times S_1\times\sqrt{\varepsilon_r}}$ (that c is the speed of light is free space and ε_r is the dielectric constant of the substrate), respectively. Based on the dimensions presented in the paper, the lowest cut off frequency is 26 GHz which much higher than the operation frequency of the antenna. Consequently, no leakage of power occurs between adjacent vias forming the cavity [27].

The optimized values of the geometrical parameters are listed in Table 1. The simulated active reflection coefficient [28], for differential feeding of the two microstrip ports, is shown in Fig. 2. This simulation shows a 10-dB return loss bandwidth of 23% centered at 5.07 GHz.

III. SINGLE-ENDED TO DIFFERENTIAL FEEDING SCHEME INTEGRATED INTO THE ANTENNA FEED NETWORK

In Section II, the antenna with differential inputs feeding the SIC was introduced. In this section, the antenna structure is modified to have a single-ended feed for the SIC while still differentially exciting the short-circuited striplines. The

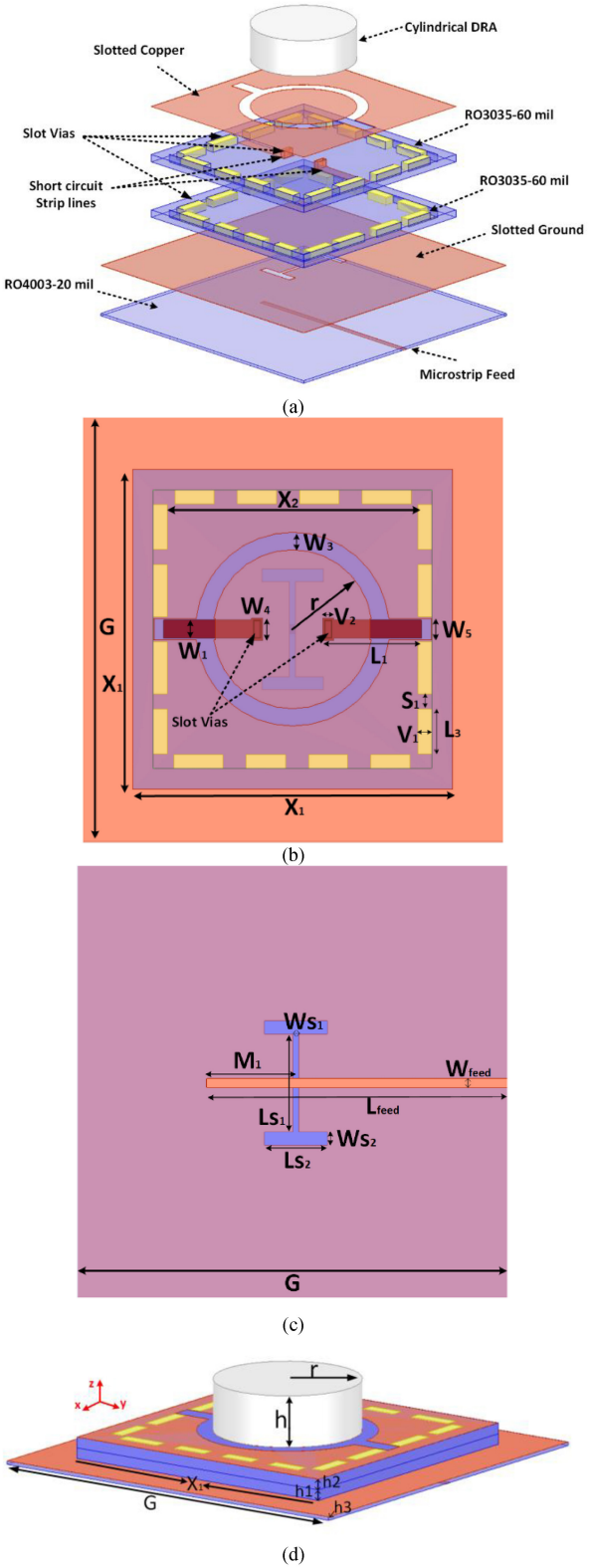

FIGURE 3. Geometry of proposed single-ended fed SIC backed cDRA (a) Disassembled view (b) Top view (c) Bottom view (d) Perspective view.

exploded view of proposed antenna is shown in Fig. 3(a). This structure eliminates the need for an external balun for exiting the antenna with a single-ended feed and so

TABLE 2. Values of different geometrical parameters in the antenna with a single port.

Parameter	Value (mm)	Parameter	Value (mm)
G	54	r	10.5
X_1	37.2	h	7.4
X_2	33.2	S_1	0.8
h_1	1.524	V_1	2
h_2	1.524	V_2	0.8
h_3	0.508	L_1	13.1
W_1	2.4	W_3	2.5
W_2	2.84	L_{feed}	35.5
W_4	2.9	L_2	8.1
W_{feed}	1.15	W_{s2}	1.7
W_{s1}	0.75	L_{s2}	8.5
L_{s1}	12.6	L_3	5

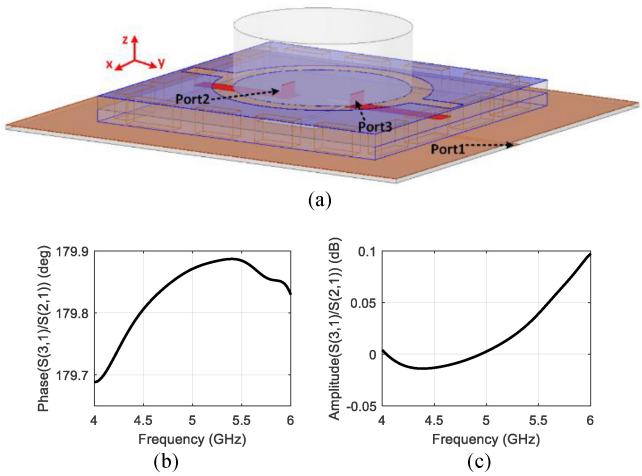

FIGURE 4. Single-ended to differential feeding conversion verification using a slot. (a) Short-circuits were replaced by ports (b) Phase difference at the location of ports (c) Amplitude ratio at the location of ports.

reduces the complexity. To differentially excite the short circuited striplines using a single-ended feed, instead of two microstrip lines that are directly connected to the short-circuited striplines (Fig. 1(a)), a slot fed by a mictorstrip line at the bottom is used (Fig. 3(c)). Here, an H- shaped slot is used to save space. The slot is at the center of the bottom metal layer of the cavity and its dimensions are specified by Ls_1, Ws_1, Ls_2, and Ws_1 as shown in Fig. 3(c) with values shown in Table 2. For feeding the slot, a 50-Ω microstrip line with width of W_{feed} and length of L_{feed} is used. Length M_1 of the open stub is used for matching purposes.

To evaluate the performance of the method in differential feeding of the short-circuited striplines, discrete ports, port 2 and port 3, were inserted at the contacts of the striplines and the vias reaching the top wall of the cavity, while the port 1 is the input of the antenna single-ended SIC feed. The phase difference and amplitude ratio of signals in the two discrete ports are shown in Fig. 4. These results show that the phase difference is close to 180° and the amplitude ratio is almost 1, which confirms the desired differential feeding behavior.

The reflection coefficients of the antenna structure with single-ended and differential feedings are compared in

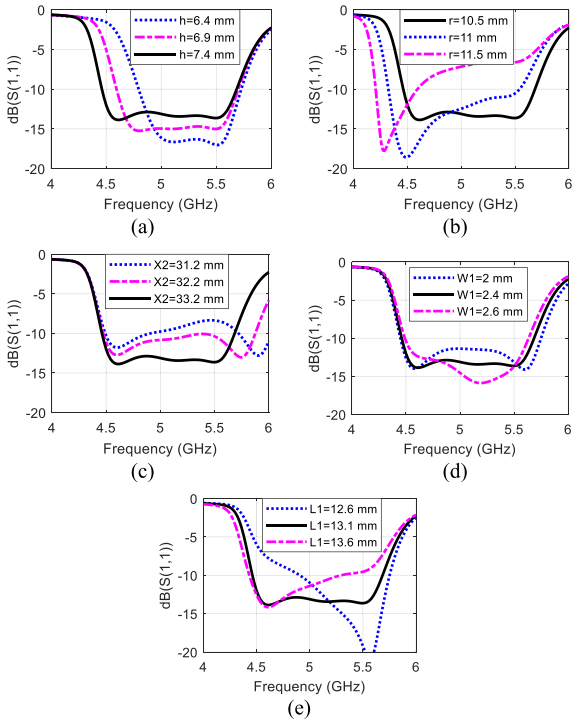

FIGURE 5. Reflection coefficient of the single-ended antenna versus frequency for different values (a) h, (b) r, (c) X_2, (d) W_1, (e) L_1. Other parameters are set according to the values provided in Table 2.

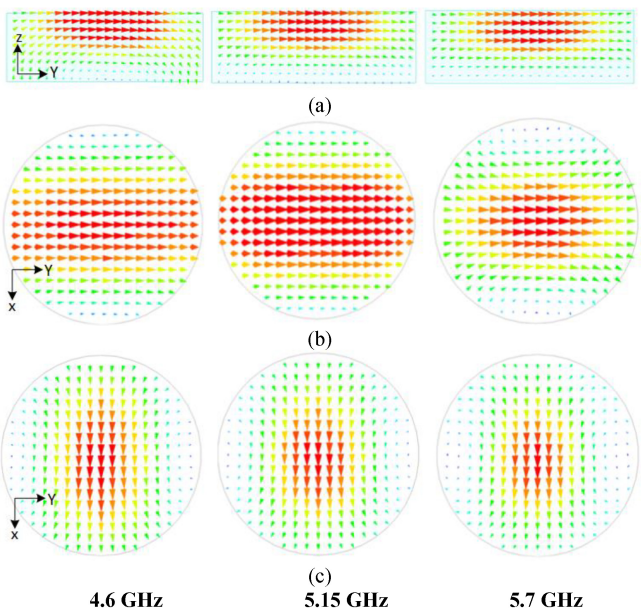

FIGURE 6. Field distributions in the cylindrical DRA antenna. (a) Side view of the electric field GHz, (b) Top view of the electric field (all electric fields are plotted within the same range of values), and (c) Top view of the magnetic field (all magnetic fields are plotted within the same range of values).

Fig. 2. Very similar performance can be observed for both antennas.

Fig. 5 shows the reflection coefficient of the antenna versus frequency for different geometrical parameters. In each figure, the other parameters are set according to the values provided in Table 2. In Fig. 5 (a) and (b), the radius (r) and height (h) of DR is changed. It shows that with changing the dimension of DR the frequency of the resonance with the lower frequency can be controlled. According to Fig. 5(c), dimension of the cavity (X_2) controls the frequency of the resonance with the higher frequency. Other parameters in Fig. 5, is related to the feed of the cavity. Based on the results shown in Fig. 5, the optimum values for different parameters are selected. Table 2 shows all final parameters.

IV. CAVITY AND DRA MODES

In order to investigate the resonant mode of the proposed cylindrical DRA, the electric and magnetic field distributions inside the DR are shown in Fig. 6 at three frequencies over the operating bandwidth (4.6, 5.15, and 5.7 GHz). In all cases, it can be observed that:

1) In Fig. 6(a), the direction of electric field distribution is in the y-direction and the amplitude shows only one peak at the top of the DR.

2) In Fig. 6(b), the electric field distribution is almost the same at the center of DRA in xy-plane.

3) In Fig. 6(c), the direction of the magnetic field is normal to the direction of the electric field at the same plane as in Fig. 6(b).

Therefore, the first two subscripts of the resonant mode corresponding to these three frequencies are identical. Based on Fig. 6, the mode of the designed DRA is $\mathrm{HEM}_{11\delta}$ [29]. It can be observed that the field distributions remain almost constant over the entire band which indicates the single-mode operation of DRA over the band. However, in Fig. 2, two different resonances can be identified from the reflection coefficients curve. The complex impedance of the input port over band (Fig. 7(a)) also confirms the existence of two resonance frequencies and one antiresonance for the antenna.

Based on dimension of SIC ($X_2 \times X_2 \times (h_1 + h_2)$), the cutoff frequency of modes inside a simple rectangular cavity can approximately be calculated from the waveguide cavity theory [26]. A simple cavity with dimensions ($X_2 \times X_2 \times (h_1 + h_2)$) specified in Table 2 supports the two modes TM_{11} and TM_{12} as their cut off frequencies are 3.4 GHz and 5.4 GHz (within the desired sub-6-GHz band), respectively. In the designed cavity and in presence of the striplines and the annular slot, field distribution of the specified modes deviates from the ones for a simple cavity. The magnetic field distribution of the modes inside the cavity are shown in Fig. 7. Looking at the magnetic field distribution inside the cavity (at the height $0.5(h_1+h_2)$ from the bottom of the cavity), we can observe two distinct modes. One is presented in Figs. 7(b) and (c) and the other is shown in the Fig. 7(d). It can be observed in Fig 7(d) that the H-filed makes a loop very close to the vias but this is not the case in the Fig. 7(b) and Fig. 7(c). According to the H-field distribution shown in the cavity ($\overline{H}_{cavity}$) in Fig. 7, $\overline{H}_{cavity}$ at the left and right of the slot is along x, that results in an equivalent electrical current $\overline{J}_{cavity}$ ($=\widehat{z}\times\overline{H}_{cavity}$) along y. According to the E-field distribution inside the DR ($\overline{E}_{DR}$) shown in Fig. 6, $\overline{E}_{DR}$ is

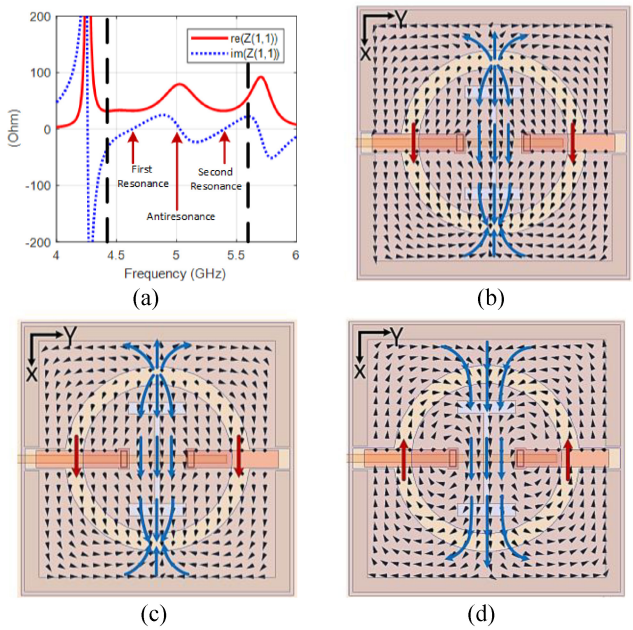

FIGURE 7. (a) Complex input impedance of the single-ended antenna over the operating band, The magnetic field distributions in the substrate cavity in different frequencies (b) 4.6 GHz, (c) 5.15 GHz, and (d) 5.7 GHz.

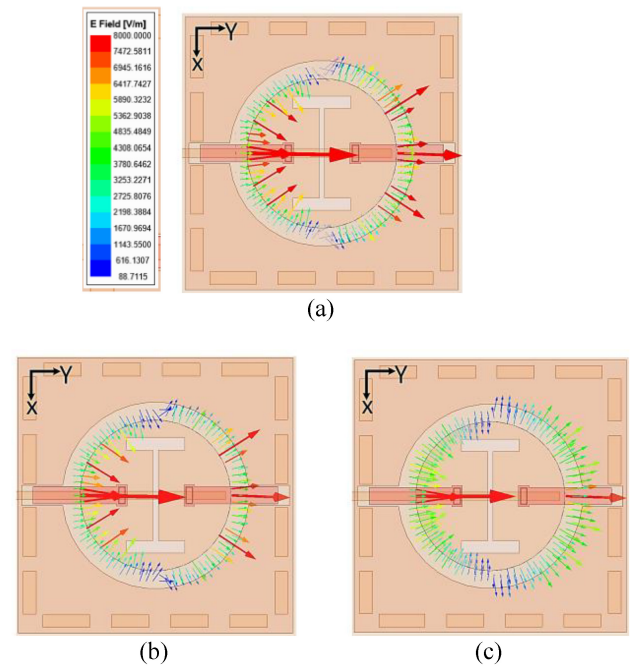

FIGURE 8. The electric field distributions in the annular slot in different frequencies (b) 4.6 GHz, (c) 5.15 GHz, and (d) 5.7 GHz (all electric fields are plotted within the same range of values).

along y. Since $\overline{E}_{DR}$ and $\overline{J}_{cavity}$ have the same direction only at the left and right part (maximum $\overline{E}_{DR} \cdot \overline{J}_{cavity}$), it can be concluded that the coupling of energy from slot to DR occurs at the left and right part of the annular slot. According to Fig. 7, though the cavity has two distinct modes, the H-field distribution ($\overline{H}_{cavity}$) at the left and right part of the slot remains along y at different frequencies within the operation

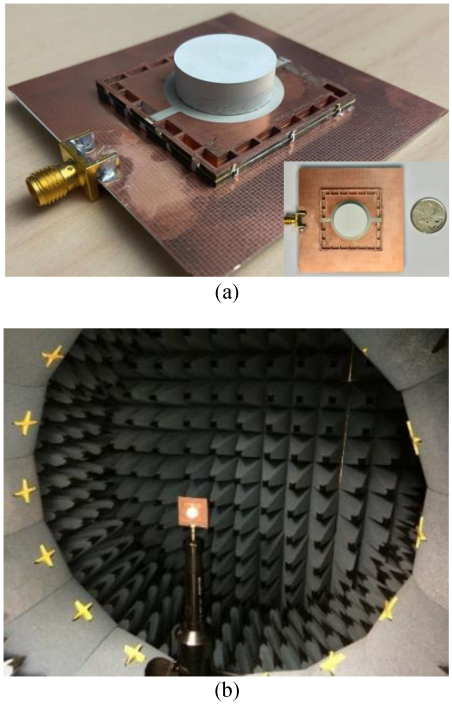

FIGURE 9. (a) Photograph of the fabricated single-ended cDRA. (b) Measurement setup.

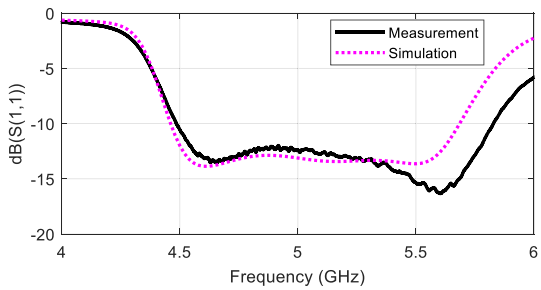

FIGURE 10. Measured and simulated reflection coefficient of the proposed single-ended cDRA.

band and so the cavity provides the similar excitation for the DR over the band (Fig. 8), resulting in single mode operation of the DR over the same band. Excitation of the two modes of the cavity results in wideband return loss bandwidth of the antenna and pure single mode wideband operation of DRA results in stable radiation characteristics (wide 1-dB gain bandwidth and low cross-polarization levels) as will be confirmed by the measurement result in the next section.

V. SIMULATION AND MEASUREMENT RESULTS FOR THE

This section presents the simulation and measurement results of the fabricated wideband cDRA with single-ended SIC feeding (Fig. 3). ANSYS HFSS was used for simulations. The antenna was tested in a Satimo Starlab near-field chamber. The fabricated antenna and measurement setup are shown in Fig. 9. The antenna was fabricated with a multi-layer fabrication process at the Poly-Grames research center

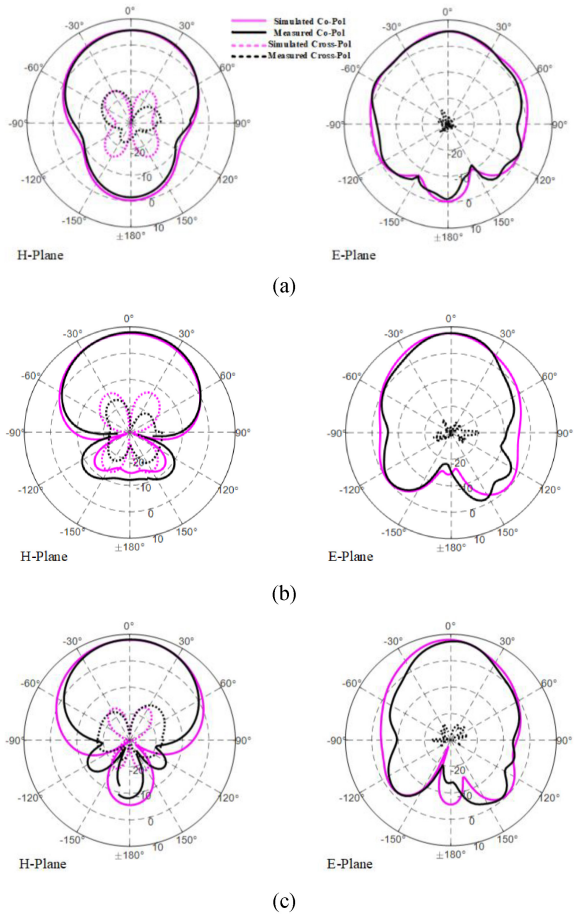

FIGURE 11. Measured E- and H-planes co-/cross polarization radiation patterns for the single-ended antenna: (a) 4.5 GHz, (b) 5.15 GHz, and (c) 5.8 GHz.

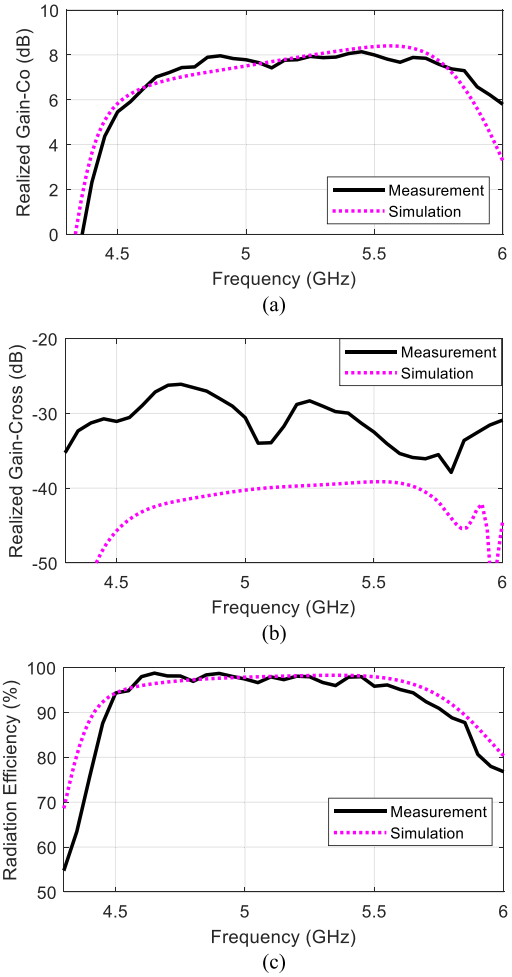

FIGURE 12. Measured and simulated (a) Realized gain-Co in broadside (b) Realized gain-Cross in broadside (c) Radiation efficiency.

at Polytechnique Montreal, and the DRA was attached via a very thin layer of epoxy glue. The measured and simulated reflection coefficients of the antenna are shown in Fig. 10. There is a very good agreement between the simulation and measurement results. The greater bandwidth for the measured curve can be attributed to the material tolerances and fabrication errors which are inevitable in such delicate designs. As seen before (e.g., Figs. 5c and 5d), small parameter variations can increase the bandwidth. Based on Fig. 10, the measured 10-dB return loss bandwidth is 26%, centered at 5.15 GHz. The measured and simulated radiation patterns of the antenna at E- and H-planes and at 4.5 GHz, 5.15 GHz, and 5.8 GHz are shown in Fig. 11. The measured and simulated results show very good agreement. Fig. 12 shows the measured and simulated realized gain and radiation efficiency versus frequency. The measured 1-dB gain bandwidth is 23% centered at 5.15 GHz. A maximum gain of 8.2 dBi is obtained at 5.45 GHz. The measured and simulated cross-polarization discrimination in the boresight direction are greater than 26 dB and 40 dB, respectively. The difference between simulated and measured cross-pol levels is mainly due to the alignment errors. Based on Fig. 12(c), the efficiency of the proposed DRA antenna is more than 95%.

A comparison of the measured performance of the proposed antenna with the previous works on single mode DRAs is presented in Table 3. Compared to the DRAs in [9], [10], [19], [20], and [21], the proposed antenna shows the largest bandwidth, lowest cross-polarization level, greatest maximum gain and smallest footprint while using a material with the same relative permittivity of 10 in all cases, except [21]. Wideband antennas are very important for multi-standard support in wireless communications. This design provides a possible solution for multi-standard coverage in wireless access point applications as it covers the bands 4.5-5.8GHz thus is suitable for different WLAN standards (802.11a/j/h/n/ac). The main part of antenna has a size of 33.2 mm $\times$ 33.2 mm (= the inner size of the cavity).

VI. CONCLUSION

A linearly polarized substrate integrated cavity-backed cDRA has been proposed for operation in the range 4.5–5.8 GHz. By using short-circuited striplines inside the cavity and differential feeding, the cavity supports two different modes to obtain a wide impedance bandwidth. Both modes provide

TABLE 3. Comparison of the measured performance of proposed DRA with the previous works with a single resonant mode.

Reference	This work	[9]	[10]	[19]	[20]	[21]
Center Frequency (GHz)	**5.15**	2.5	2.38	23.7	3.73	2.43
1-dB Gain Bandwidth (%)	**23**	~19	-	-	-	~18
BW (|S11|<-10 dB) %	**26**	22	9.2	3.2	7	18.1
Permittivity of DR	**10**	10	10	10.2	10	6.85
Maximum Gain (dBi)	**8.2**	6.6	6.32	7	6.45	2.04
Cross-pol. level (dB)	**< -26**	< -15	< -24	< -18	< -20	< -13
External Balun	**No**	Yes	Yes	Yes	No	Yes
Antenna Size ($*/\lambda_0^3$)	**0.65 × 0.65 × 0.19**	1 × 0.83 × 0.22	0.79 × 0.79 × 0.31	-	0.75 × 0.75 × 0.21	$\pi \times 0.53^2 \times 0.21$
Resonant mode	**HEM11δ**	TEδ11	HEM11δ	TE111	TE111	TE011δ

*λ_0 is the free-space wavelength at the center frequency

the same exciting fields for the DRA to excite the singe $HEM_{11\delta}$ mode that results in stable radiation characteristics (gain pattern and polarization) for the antenna over the operation bandwidth. Compared to the previous single-mode DRAs (Table 3), the proposed antenna shows the largest 1-dB gain and 10-dB impedance bandwidth. Measurement results show the largest 10-dB impedance (26%) and 1-dB gain bandwidth (23%) compared to the previous single mode DRAs. This cannot be achieved with a simple single slot excitation. The cavity is differentially excited by either differential feeding or an embedded single-ended to differential converter to eliminate the need for an external balun.

REFERENCES

[1] S. Long, M. McAllister, and L. Shen, "The resonant cylindrical dielectric cavity antenna," *IEEE Trans. Antennas Propag.*, vol. 31, no. 3, pp. 406–412, May 1983.

[2] G. Das, N. K. Sahu, A. Sharma, R. K. Gangwar, and M. S. Sharawi, "Dielectric resonator-based four-element eight-port MIMO antenna with multi-directional pattern diversity," *IET Microw. Antennas Propag.*, vol. 13, no. 1, pp. 16–22, 2018.

[3] Y. M. Pan and S. Y. Zheng, "A low-profile stacked dielectric resonator antenna with high-gain and wide bandwidth," *IEEE Antennas Wireless Propag. Lett.*, vol. 15, pp. 68–71, 2016.

[4] X.-Y. Wang, S.-C. Tang, L. L. Yang, and J.-X. Chen, "Differential-fed dual-polarized dielectric patch antenna with gain enhancement based on higher order modes," *IEEE Antennas Wireless Propag. Lett.*, vol. 19, pp. 502–506, 2020.

[5] K. W. Leung, K. M. Luk, E. K. N. Yung, and S. Lai, "Characteristics of a low-profile circular disk DR antenna with very high permittivity," *Electron. Lett.*, vol. 31, pp. 417–418, Mar. 1995.

[6] X. S. Fang, K. P. Shi, and Y. X. Sun, "Design of the single-/dual-port wideband differential dielectric resonator antenna using higher order mode," *IEEE Antennas Wireless Propag. Lett.*, vol. 19, pp. 1605–1609, 2020.

[7] Y. X. Sun and K. W. Leung, "Dual-band and wideband dual-polarized cylindrical dielectric resonator antennas," *IEEE Antennas Wireless Propag. Lett.*, vol. 12, pp. 384–387, 2013.

[8] T.-Y. Lin, T. Chiu, and D.-C. Chang, "V-band dual-polarised dielectric resonator antenna with bondwire feeding structures," *Electron. Lett.*, vol. 53, no. 12, pp. 764–766, 2017.

[9] S.-J. Guo, L.-S. Wu, K. W. Leung, and J.-F. Mao, "Microstrip-fed differential dielectric resonator antenna and array," *IEEE Antennas Wireless Propag. Lett.*, vol. 17, pp. 1736–1739, 2018.

[10] Y.-X. Sun, K. W. Leung, and J.-F. Mao, "Dualfunction dielectric resonator as antenna and phase-delay-line load: Designs of compact circularly polarized/differential antennas," *IEEE Trans. Antennas Propag.*, vol. 66, no. 1, pp. 414–419, Jan. 2018.

[11] A. A. Kishk, X. Zhang, A. W. Glisson, and D. Kajfez, "Numerical analysis of stacked dielectric resonator antennas excited by a coaxial probe for wideband applications," *IEEE Trans. Antennas Propag.*, vol. 51, no. 8, pp. 1996–2006, Aug. 2003.

[12] Y.-X. Guo and K.-M. Luk, "On improving coupling between a coplanar waveguide feed and a dielectric resonator antenna," *IEEE Trans. Antennas Propag.*, vol. 51, no. 8, pp. 2144–2146, Aug. 2003.

[13] W. M. Abdel-Wahab, D. Busuioc, and S. Safavi-Naeini, "Millimeter-wave high radiation efficiency planar waveguide series-fed dielectric resonator antenna (DRA) array: Analysis, design, and measurements," *IEEE Trans. Antennas Propag.*, vol. 59, no. 8, pp. 2834–2843, Aug. 2011.

[14] H. Tang, X. Deng, and J. Shi, "Wideband substrate integrated differential dual-polarized dielectric resonator antenna," *IEEE Antennas Wireless Propag. Lett.*, vol. 21, pp. 203–207, 2022.

[15] Q. Lai, C. Fumeaux, W. Hong, and R. Vahldieck, "60 GHz aperture-coupled dielectric resonator antennas fed by a half-mode substrate integrated waveguide," *IEEE Trans. Antennas Propag.*, vol. 58, no. 6, pp. 1856–1864, Jun. 2010.

[16] Q. Xue, X. Y. Zhang, and C.-H. K. Chin, "A novel differential-fed patch antenna," *IEEE Antennas Wireless Propag. Lett.*, vol. 5, pp. 471–474, 2006.

[17] X. S. Fang, K. W. Leung, E. H. Lim, and R. S. Chen, "Compact differential rectangular dielectric resonator antenna," *IEEE Antennas Wireless Propag. Lett.*, vol. 9, pp. 662–665, 2010.

[18] H. Tang, J.-X. Chen, W.-W. Yang, L.-H. Zhou, and W. H. Li, "Differential dual-band dual-polarized dielectric resonator antenna," *IEEE Trans. Antennas Propag.*, vol. 65, no. 2, pp. 855–860, Feb. 2017.

[19] C.-W. Tong, H. Tang, J. Li, W.-W. Yang, and J.-X. Chen, "Differentially coplanar-fed filtering dielectric resonator antenna for millimeter-wave applications," *IEEE Antennas Wireless Propag. Lett.*, vol. 18, pp. 786–790, 2019.

[20] Y. Gao, Z. Feng, and L. Zhang, "Compact CPW-fed dielectric resonator antenna with dual polarization," *IEEE Antennas Wireless Propag. Lett.*, vol. 10, pp. 544–547, 2011.

[21] X. Liu, K. W. Leung, and N. Yang, "Wideband horizontally polarized omnidirectional cylindrical dielectric resonator antenna for polarization reconfigurable design," *IEEE Trans. Antennas Propag.*, vol. 69, no. 11, pp. 7333–7342, Nov. 2021.

[22] G. Q. Luo, Z. F. Hu, L. X. Dong, and L. L. Sun, "Planar slot antenna backed by substrate integrated waveguide cavity," *IEEE Antennas Wireless Propag. Lett.*, vol. 7, pp. 236–239, 2008.

[23] G. Q. Luo, Z. F. Hu, L. X. Dong, and L. L. Sun, "Circularly polarized antenna based on dual-mode circular SIW cavity," presented at the ICMMT 2008.

[24] S. Hashemi-Yeganeh and C. Birtcher, "Theoretical and experimental studies of cavity-backed slot antenna excited by a narrow strip," *IEEE Trans. Antennas Propag.*, vol. 41, no. 2, pp. 236–241, Feb. 1993.

[25] R. K. Mongia and P. Bhartia, "Dielectric resonator antennas—A review and general design relations for resonant frequency and bandwidth," *Int. J. Microw. Millimeter-Wave Comput.-Aided Eng.*, vol. 4, pp. 230–247, Jul. 1994.

[26] D. M. Pozar, *Microwave Engineering*, 2nd ed. New York, NY, USA: Wiley, 1998.

[27] A. B. Numan, J.-F. Frigon, and J.-J. Laurin, "W-band compact slot antenna arrays with polarization flexibility," *Radio Sci.*, vol. 53, no. 6, pp. 739–748, Jun. 2018.

[28] R. C. Hansen, *Phased Arrays Antennas*. Hoboken, NJ, USA: Wiley, 2009, ch. 7, p. 224.

[29] D. Kajfez, A. W. Glisson, and J. James, "Computed modal field distributions for isolated dielectric resonators," *IEEE Trans. Microw. Theory Techn.*, vol. 32, no. 12, pp. 1609–1616, Dec. 1984.

REZA SHAMSAEE MALFAJANI (Graduate Student Member, IEEE) received the B.S. degree in electrical engineering from the University of Tehran, Tehran, Iran, in 2009, and the M.S. degree in electrical engineering from Tarbiat Modares University, Tehran, in 2012. He is currently pursuing the Ph.D. degree with Polytechnique Montréal, Montreal, QC, Canada, where he is also a member of the Poly-Grames Research Center. His research focuses on the periodic structures, antennas and RF, mm-wave, and terahertz designs.

JEAN-JACQUES LAURIN (Senior Member, IEEE) received the B.Eng. degree in engineering physics from the Ecole Polytechnique de Montréal, Montreal, QC, Canada, in 1983, and the M.A.Sc. and Ph.D. degrees in electrical engineering from the University of Toronto, Toronto, ON, Canada, in 1986 and 1991, respectively. In 1991, he joined the Poly-Grames Research Centre, Ecole Polytechnique de Montréal, where he is currently a Professor. He is the Co-Director of STARaCom (Center for Systems, Technologies and Applications for Radiofrequency and Communications), a strategic research cluster in the province of Quebec. His research interests include antenna design and modeling, wave processing surfaces, near-field antenna measurement techniques, and electromagnetic compatibility.

MOHAMMAD S. SHARAWI (Senior Member, IEEE) is a Full Professor with the Electrical Engineering Department, the University of Montréal (Polytechnique Montréal), Quebec, Canada, where he is also a member of the Poly-Grames Research Center. He was with the King Fahd University of Petroleum and Minerals, Dhahran, Saudi Arabia, from 2009 to 2018, where he founded and directed the Antennas and Microwave Structure Design Laboratory. He was a Visiting Professor with the Intelligent Radio Laboratory, Department of Electrical Engineering, University of Calgary, Calgary, AB, Canada, in Summer–Fall 2014. He was a Visiting Research Professor with Oakland University, Rochester, MI, USA, in Summer 2013. He has more than 350 papers published in refereed journals and international conferences, 11 book chapters (two of which in the Antenna Handbook, 5th edition, McGraw Hill, 2018), one single authored book titled *Printed MIMO Antenna Engineering* (Artech House, 2014), and the Lead Author of the recent book *Design and Applications of Active Integrated Antennas* (Artech House, 2018). He has 28 issued/granted and nine pending patents in the U.S. Patent Office. His research interests include multiband printed multiple-input-multiple-output (MIMO) antenna systems, reconfigurable and active integrated antennas, millimeter-wave MIMO antennas and integrated 4G/5G antennas, microwave sensors, applied electromagnetics, and computational methods. He was a recipient of the Abdul Hameed Shoman Foundation Award for Arab researchers for the category of wireless systems in 2020 in addition to various best IEEE Conference Paper Awards. He is also serving as an Associate Editor for the IEEE ANTENNAS AND WIRELESS PROPAGATION LETTERS, *IET Microwaves, Antennas and Propagation*, and IEEE OPEN JOURNAL ON ANTENNAS AND PROPAGATION; and an Area Editor (Antennas and Microwave Devices and Systems) *Microwave and Optical Technology Letters* (Wiley). He was the Specialty Chief Editor for the newly launched *Frontiers in Communications and Networks* for the System and Test-Bed Design Section. He has served on the technical and organizational program committees and organized several special sessions on MIMO antenna systems and architectures in several international conferences, such as EuCAP, APS, IMWS-5G, APCAP, and iWAT among many others for many years. He is also the IEEE Antennas and Propagation Society Chair of the Montreal section and an Active Member of the IEEE Member Benefits Committee leading the initiative of the APS Student Travel Grant. He is also the Regional Delegate of the EuRAAP in North America. He is a Distinguished Lecturer of the IEEE Antennas and Propagation society from 2023 to 2025.